Investigation using Monte-Carlo codes simulations for the impact of temperatures and high pressures on thin films quality

A. Bouazza
L2GEGI Laboratory, University of Tiaret, 14000 Tiaret, Algeria.

Received 10 May 2022; accepted 16 August 2022

The quality of thin films is the key to any improvement made in the manufacturing of device components. Therefore, the method of obtaining this quality based on the deposition parameters is the focus of our group. The influence of temperature and high pressure on the number of ejected particles, and therefore their deposition and formation of the finest thin films, is investigated in this paper using the sputtering technique in the context of the Monte-Carlo approximation. First, a vacuum chamber with a dimension of $30 \times 30 \times 50$ cm, holding a magnetron with a circular target with a radius of 2 cm, was created. Then, inside this chamber, 10^5 particles of argon (Ar) were followed by the same amount of xenon (Xe) gas we injected. This target moves 8 cm away from the substrate (with a radius of 7 cm), containing three materials (silicon (Si), germanium (Ge), and copper (Cu)) widely used in advanced technologies such as electronics and photovoltaic cell panels. The obtained results demonstrate that increasing the pressure (0.5, 2, and 5 Pa) for both gases dropped off spectacularly the total number (with different values) of the material particles reaching the substrate and disrupting the morphology of thin films. Moreover, in contrast to pressure, it has also been proven that mounting gas temperatures of 100, 300, and 600 K, representing three different states in Kelvin degrees, where 100 K $\approx$ -173°C for the low (cold), 300 K $\approx$ 27°C for the regular (atmospheric), and 600 K $\approx$ 327°C for the high (warm) instances, supply a large number of material atoms at the substrate level. In addition, silicon yielded the best results compared to germanium and copper.

Keywords: Thin film; PVD process; sputtering technique; plasma.

DOI: https://doi.org/10.31349/RevMexFis.69.021501

1. Introduction

Modern technologies and their components, such as cell phones, laptops, and smartwatches, rely on cutting-edge technology to be manufactured. Therefore, they typically require small parts obtained from miniaturized wafers using thin-film technology [1–5].

In 1912, Pohl and Pringsheim accomplished thin films. They published a famous work on the production of mirrors using a process of metal vaporization such as silver (Ag) and aluminum (Al) in a high vacuum [6–8]. Later, with research and development in this field, the application of this domain was seen in the semiconductor industry, which represents the primary manufacturing technology, including telecommunication apparatus, integrated circuits (IC), transistors, solar cells, LEDs, photoconductors, magneto-memory optics, compact discs, and so on [9–12].

Several methods can be used to perform these miniaturization techniques where the sputtering process under the physical vapor deposition (PVD) system presents powerful results. For example, the magnetron sputtering technique allows metallic or non-metallic layers to be deposited on the substrate. Using a magnetron associated with the cathode creates a magnetic field that imposes the trajectories of the ejected electrons from the target, expanding the bombardment density [13–16].

Various simulation programs have been used to simulate the sputtering deposition process. Ready to cite an effective program based on the Monte-Carlo simulations SRIM [17].

During the simulation, the particle moved in a sequence of discrete steps, each of which collided with an atom of the target in an arbitrary mode, reproducing the statistical properties of the shutdown processes [18–20]. The composition development of binary thin films takes place experimentally and with Monte Carlo codes based on TRIDYN (DYNamic TRAnsport of Ions in the matter) [21] and TRIM (TRansport Ions in Matter) [17]. Another code, SIMTRA [22], was developed by Van Aeken for the trajectory simulation of gas-phase particles in a definable 3D configuration. The background molecules' interatomic collision modeling, potentials, and thermal movement are included in the code [23–25].

The morphology of the layers deposited via the sputtering method relies on the material, vacuum chamber gas, and numerous deposition parameters, such as pressure, target-substrate distance, temperature, substrate bias, and chemical composition [26, 27].

Deposition using the sputtering approach is a complex task; it is suitable for creating a process model for acquiring the physical values of sputtering. We used a model to simulate the sputtering and transport processes, as in our previous work [1–5].

It is widely known that the properties of thin-film materials depend on their sputtering state. However, the relationship between the plasma parameters of sputtering and the properties of thin films is unclear. The optimal sputtering conditions must be determined by preparing many samples under varying sputtering parameters. The results obtained

help understand the effect of process parameters on transport, the sputter deposition process, and the resultant composition of films.

Several experimental studies have been conducted [28–31] showing the relationship between sputter deposition parameters and the quality of thin films obtained, thus validating the simulation models.

Previous works by different groups [32–34] do not permit target properties when utilizing metals, semiconductors, and dielectrics. Their posted results, primarily based on Monte Carlo models, are typically speaking, although it is imperative to recognize the distinction in using each. Furthermore, other groups [35–37] have demonstrated a close relationship between the transport conditions of the particles from the target to the substrate and their arrival energies.

Before deposition, the sputtered atoms underwent various binary collisions with plasma particles. This amount is vital because each collision induces a trajectory and energy variation. Therefore, the collisions with the background gas atoms were disregarded relative to the sputtered particles' critical number of kinetic energies.

The morphology and quality of thin-film materials depend highly on the sputtering conditions. However, our group intends to examine the link between thin-film properties and plasma parameters. Thus, in earlier research cited in Refs. [1-3], we have shown the following:

A. In Ref. [1]: The simulation results obtained from a Monte Carlo code based on experimental and algorithmic calculations have been compared with those of other authors like Mahieu *et al*. [38]. They applied a Monte Carlo code to simulate the transport of atoms in DC magnetron sputtering, studied the thickness profiles, and simulated the power and path of sputtered particles arriving at the substrate.

Results: Target-substrate distances of $8-20$ cm and a 0.3-1 Pa pressure range correspond well with the results above.

B. In Ref. [2]: The results acquired with analytical formulation primarily based on the Monte Carlo approach proposed by researchers such as Sigmund and Yamamura were compared with SRIM code simulation to validate models.

Results: The Yamamura model and SRIM simulation approximated the sputtering yield rate, mainly when no experimental data were available. SRIM was validated for energies above 100 eV but is not appropriate for less than this value.

C. In Ref. [3], the simulation results using the Monte Carlo code of the sputtering yield for metals and semiconductors were obtained by varying the energy and angles of incidence.

Results: As many ejected particles ensure a very thin and uniform film deposition, which we are looking forward to obtaining, we deduced the optimum energy and angle that should be applied in this way.

The present work studied the influence of two other parameters, temperature, and high pressure, on the sputtering process for silicon, germanium semiconductors, and copper metal. Continuing this goal, we started in our previous work by providing the necessary information through simulation and analytical computation, including all parameters that affect the desired thin-film realization that can be considered in experimental research or industry.

2. The sputtering process requirements

It is vital to understand the steps of the reactor equipment process to achieve a better deposition morphology of thin films, considering what occurs inside the vacuum chamber during the disposition cycle. Therefore, a preparation process was required before the deposition. Before its placement, cleaning the substrate outside the vacuum chamber in an ultrasonic bath resulted in outstanding film adhesion. This technique transforms electrical power into mechanical vibrations within a cleaning liquid. It is quick and less expensive because it does not require too much solvent and is easier to handle than an ionic bath [39–41].

The cleaning procedure takes a long time, which is a disadvantage in terms of industry efficiency because it boosts the final product costs. Controlling expenses requires managing the breakdown times and setup of the machine. Because this is a disadvantage to the industry, process parameter optimization is essential for reducing production times. The deposition rate is an important parameter that must be tuned to enhance the plasma density and energy available in the process. Therefore, it is necessary to consider all steps and parameters being studied to comply with the industry demands [42]. Furthermore, to obtain significant sputtering, it is necessary to go through the steps depicted in the following:

- The first step (adjustment) consisted of preparing the vacuum chamber, which is composed of a gradual increase in temperature created by tubular heating and a modular control system. Simultaneously, vacuum pumps were activated to reduce the pressure inside the chamber. For this, two pumps are used; the first produces a pressure of up to 10-5 bar, and the second (high vacuum) creates a pressure of $10-7$ bar.

- The second step (engraving) is characterized by cathode cleaning, where the substrate is bombarded with ions from plasma etching to remove localized contamination on the substrate surface. This step is crucial before starting sputtering because it helps to increase adherence.

- Third step (gas integration): Before starting, we must integrate a gas that aims to bombard our target. Several gas choices are available, such as argon and xenon; the

choice of gas is significant because it contributes to the sputtering efficiency.

– In the fourth step (coating), the sputtering process is started, and the material to be deposited is projected onto the substrate surface.

– The final step (ramp down) corresponds to the cooling of the chamber; a specific system must be applied to return the vacuum chamber to room temperature and ambient pressure [43–45].

3. Simulation protocol

The development of simulation models for sputtering with appropriate physical parameters can reduce time-consuming and costly trials in the operation and control of deposition systems used to fabricate thin films.

The simulation of film growth on time scales of seconds or minutes is possible using kinetic Monte Carlo algorithms [46,47].

This approach can model different surface processes such as nucleation, growth, post-deposition, and structural modification of films [48,49].

3.1. Simulation codes

The Sigmund-Thompson distribution describes the initial energy distribution well; the angular distribution of the sputtered particles is considered as $\cos^{n}(\theta)$ type (θ is the emission angle of the sputtered particle with respect to the surface normal) depending on the incidence angle and energy of the impinging particle.

The kinetic energy and the number of atoms arriving at the substrate were calculated using SRIM and SIMTRA.

The simulation was divided into two parts:

– The main goal of the first part is to calculate the sputtering yield $Y(E)$ using the Monte Carlo simulation program SRIM, which uses the binary collision approximation (BCA) applied to ion-solid interactions [17]. This is an open-source program that is convenient for practical use.

Different angles of incidence were used (θ = [0°, 15°, 30°, 45°, 60°, 75°, 85°, and 89°]), and the sputtering yield was varied according to the applied energy (E = [100 eV, 1 KeV, 10 KeV, 100 KeV, and 1000 KeV]), and the target was bombarded by the vacuum chamber gas ions (argon and xenon) using the materials (Si, Ge , and Cu).

Each material must consider the incidence angle and bombardment energy to obtain the optimum results. Therefore, we note the bombardment energy and the incidence angle, which give the highest sputtering yield, named $E_{\max}$ and $\theta_{\max}$, respectively. These two parameters represent the maximum number of ejected atoms extracted from the target.

– The transport from the target to the substrate of the sputtered atoms (obtained from the sputtering yield calculation by applying $E_{\max}$ and $\theta_{\max}$) is then handled by the SIMTRA code in the second part [50,51], considering all collisions occurring in the gas phase.

Diverse temperatures (T = [100, 300, and 600 K]) and pressures (P = [0.5, 2, and 5 Pa]) were applied. The first parameter represents the three temperature states of the vacuum chamber in Kelvin, where 100 K ≈ -173°C for the low (cold), 300 K $\approx$ 27°C for the normal (atmospheric), and 600 K $\approx$ 327°C for the high (warm) instances. The same applies to the second parameter, from low to high pressure. At the end of the simulation, SIMTRA will give us a file of results containing the number of atoms that arrived on the substrate, with their energies and positions.

The main objective was to determine the effect of these two parameters on the number and energy of atoms that have reached the substrate. Moreover, deduce the temperature and pressure that should be applied to acquire the maximum number of atoms and hence the desired thin films.

3.2. Simulation model

As is most commonly used in industrial applications, we created a vacuum chamber with dimensions of $30 \times 30 \times 50$ cm, a distance of 8 cm between the target and substrate, a circular shape of 2 cm in the magnetron target's radius, and 7 cm in the substrate radius (as shown in Fig. 1).

Using SRIM, we injected approximately 10^5 argon and xenon ions intended to bombard with the Eopt of energy and θ_{opt} as the incidence angle on the three different targets: Si, Ge, and Cu. The best choice of bombardment gas factors is crucial for guaranteeing the optimum layer morphology.

The gas temperature and pressure were varied to determine their influence on the number of atoms reaching the substrate and their energies.

After these configurations, we can start the simulation of this model to calculate the total number of particles arriving at the substrate, their positions, and their energies. The results were saved to data files and represented as curves.

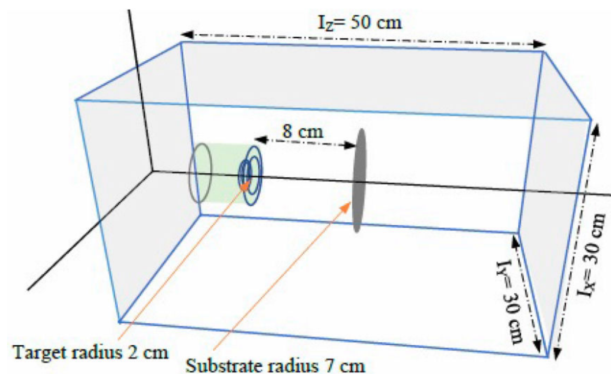

FIGURE 1. The model used in the simulation.

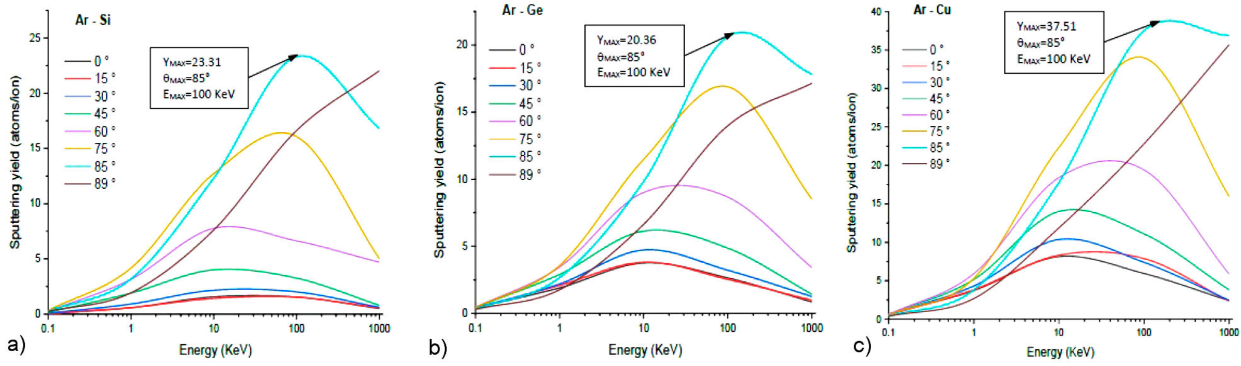

FIGURE 2. Sputtering yield as a function of the energy of the bombardment ions (Ar) for various incidence angles calculated by the MC method for a) Si, b) Ge, and c) Cu materials.

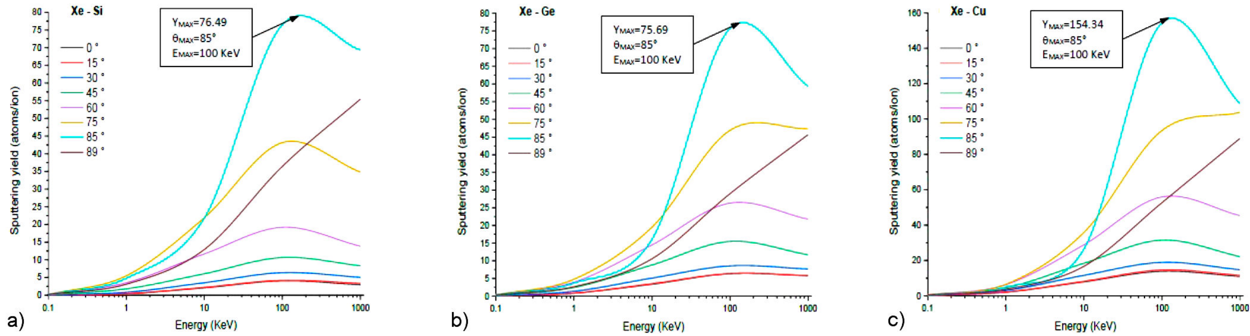

FIGURE 3. Sputtering yield as a function of the energy of the bombardment ions (Xe) for various incidence angles calculated by the MC method for a) Si, b) Ge, and c) Cu materials.

4. Results and discussion

4.1. Sputtering yield calculation

The sputtering process involves momentum transport in a collision cascade initiated by the incident particles in the solid surface layer. A surface atom is ejected if its energy exceeds its surface binding energy. To evaluate the number of atoms ejected under ion bombardment, we calculated the sputtering yield $Y(E)$, which quantifies physical sputtering and is defined as the mean number of atoms removed from the surface of a solid per incident ion [2–4, 52].

$$Y(E) = \frac{\text{emitted atoms number}}{\text{projectiles number}}.$$

4.1.1. Sputtering yield depends on the bombardment energy and incidence angles

Figures 2 and 3 below represent sputtering yield rates obtained with SRTM code simulation for Si, Ge, and Cu materials bombarded with Ar and Xe vacuum chamber plasma gas, applying different energy and incidence angle values.

By looking at these two Figs. 2 and 3), we can deduce those observations:

1. Bombarding with Xe ions yielded a better sputtering yield than bombarding with Ar ions. Xe offers approximately 4-fold sputtered atoms compared to Ar and those for metals and semiconductors.

2. At [100 KeV/ 85°], for both Ar and Xe gases, the sputtering yield reached the maximum value, which represents the supreme value of the ejected atoms obtained from the sputtering process for different materials (Si, Ge, and Cu)

4.1.2. Comparison between different materials

In Fig. 4, we present the curve results of the sputtering yield calculations obtained by SRIM simulations. At an incidence angle of 85°, the sputtering yield varied according to the energy, and the target was bombarded with argon and xenon ions using the materials (Si, Ge, and Cu).

As illustrated in Fig. 4, increasing the bombardment energy created a peak called $Y_{\max}$ at 100 KeV of applied energy, and surpassing this value reduced the sputtering yield for each material employed.

Copper is an excellent conductor, whereas germanium and silicon are semiconductors. Thus, the resistance of copper decreases, but that of germanium and silicon increases when they are subjected to an increase in the energy of the gas bombardment ions, which influences the atomic bond and leads to a significant difference between the ejected particles of metal (Cu) and semiconductors (Ge and Si).

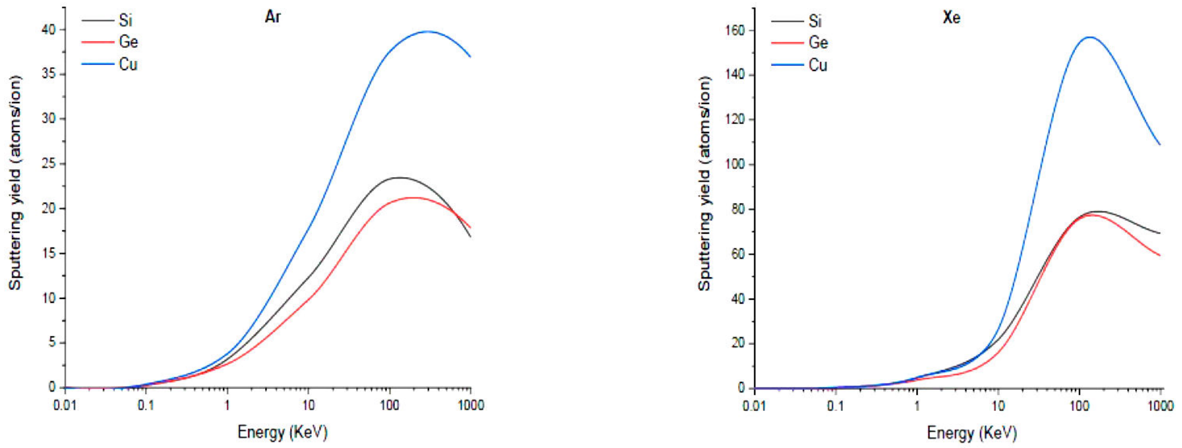

FIGURE 4. Comparison of sputtering yield on 85° of incidence angle as a function of the energy of the argon and xenon bombardment ions.

The following regions can be developed for these curves:

- In region 1, sputtering at low energy (subthreshold): in this region, which covers the energy range from 0 to 80 eV, the bombardment energy is insufficient for the sputtering process to begin because either the argon or xenon ions have insufficient energy to reach the target or their energies are below the surface binding energy of the cathode materials.
- In region 2, knock-on sputtering, commercial and industrial sputtering applications are most interested in ions with energies in this region (approximately between 100 eV and one keV). The sputtering process began when the bombardment energy reached a threshold. Furthermore, the surface and near-surface atoms can be energetically removed from their equilibrium locations once the energy of the sputtering ions exceeds the surface binding energy of the cathode material. Increasing the bombardment energy accelerates this process. This area is known as the liner cascade regime [53–55].
- In region 3, nonlinear cascade sputtering appeared for ions with threshold energies above one keV. The incident ions are sufficiently strong to remove several cathode atoms. At approximately $80 - 100$ KeV, the sputtering process reaches its limit. In this situation, the ions have high energy, and the striking particles penetrate deeply into the target, preventing the recoil atoms from escaping. Therefore, the addition of more energy reduced the yield. This regime is often not of industrial interest because of the high energy required and the high ejection energies of sputtered atoms.

Typical operating voltages used in commercial and industrial sputtering applications are between 100 eV and one keV [53-55]. Therefore, $E_{\text{opt}} = 1$ KeV was selected as the optimal energy source. This is justified by the previous Figs. 2-4, where the best value for the sputtering yield in this region could be registered. Furthermore, $\theta_{\text{opt}} = 75°$ was the optimal incidence angle corresponding to the sputtering yield for both gases (see Table I).

Thus, we take the optimal values to $\theta_{\text{opt}} = 75°$ and $E_{\text{opt}} = 1$ KeV to consider them as the default incidence angle and energy entrance parameters for the SIMTRA program (as this code offers the opportunity to do) and launch the simulation for the transport of these ejected particles with variations in temperature and pressure, respectively.

TABLE I. Sputtering yield for 1 KeV of the energy of the bombardment ions (Ar and Xe) as a function of various incidence angles calculated by the MC method for Si, Ge, and Cu materials.

		Sputtering Yield							
		0 Deg	15 Deg	30 Deg	45 Deg	60 Deg	75 Deg	85 Deg	89 Deg
Ar	Si	0.5822	0.582	0.914	1.9	3.15	4.17	3.18	1.93
	Ge	1.89	2.08	2.18	2.89	3.44	3.56	2.65	1.75
	Cu	3.71	3.83	4.31	5.15	5.91	5.29	3.79	2.67
Xe	Si	0.399	0.404	0.807	1.79	3.5	5.48	4.76	3.07
	Ge	0.834	0.84	1.38	2.45	3.96	4.78	3.7	2.66
	Cu	2.04	2.07	3	4.51	6.25	6.46	4.86	3.61

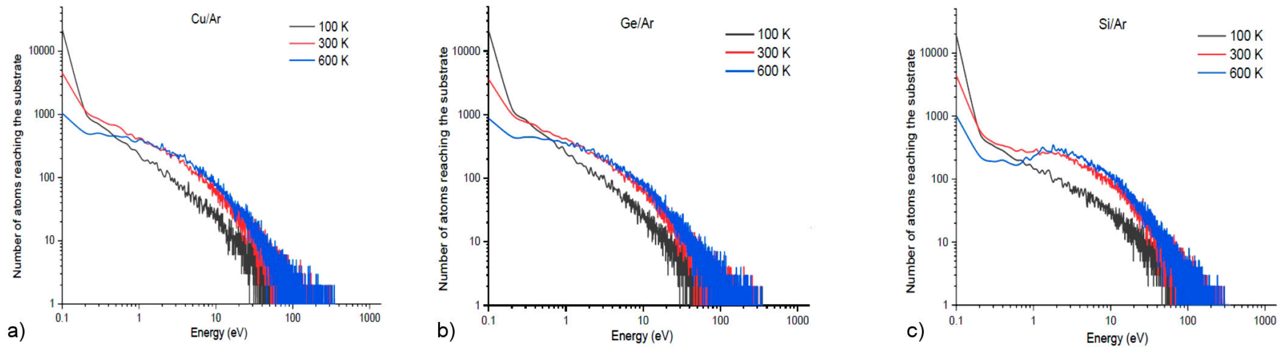

FIGURE 5. Number of arriving atoms as a function of the atom's kinetic energy for three different temperatures $T =$ [100, 300, and 600 K] with Argon gas bombardment for a) Cu, b) Ge, and c) Si.

4.2. Influence of temperature and high pressure on the sputtered atoms arriving on the substrate using argon and xenon gas

4.2.1. Variation of temperature with a fixed pressure for argon ions

In the vacuum chamber, the target, which contains materials (Si, Ge, and Cu), is bombarded with argon gas ions with the optimal values of incidence angle and energy obtained from the SRIM simulation (75° and 1 KeV).

When the chosen pressure is 0.5 Pa, and with the temperature variation (100, 300 , and 600 K), the following figures represent the number of atoms that arrive on the substrate for each considered temperature, obtained with SIMTRA code simulation.

As shown in Fig. 5a), b), and c), the number of atoms that reached the substrate was different at each adjusted temperature. For example, when 100 K was applied, the total number of Si, Ge, and Cu atoms reaching the substrate was approximately 38000, 34000, and 37000, respectively. Applying 300 and 600 K increased the mobility and energy of the argon gas particles, bombarding the target with great energy on one side and expanding the number of ejected atoms on the other side (Table II).

TABLE II. The total number of material atoms arrived in the substrate depending on temperature with argon gas ions bombardment.

Temperature	Materials	Total number of atoms
100 **K**	Si	38315
	Ge	33914
	Cu	37520
300 **K**	Si	39146
	Ge	35549
	Cu	36177
600 **K**	Si	41886
	Ge	37315
	Cu	38520

4.2.2. Variation of pressure with a fixed temperature for Argon ions

In this section, we investigate the effect of high pressure by applying three different pressures (0.5, 2, and 5 Pa) while maintaining the temperature inside the vacuum chamber at 100 K. Using the same gas (argon) and materials (Cu, Ge, and Si) to bombard the target, and the obtained results are presented in the Fig. 6.

According to the above graphs (Fig. 6 a), b), and c)), the pressure significantly influences the number of atoms arriving at the substrate. When 0.5 Pa was applied, approximately 38000, 34000, and 37000 arriving atoms for Si, Ge, and Cu were obtained.

Enlarging the vacuum chamber pressure to higher values produces many collisions and a massive drop in particle mobility. The ejected atoms collide with the argon ions, which decreases their kinetic energy and makes it difficult for them to reach the substrate. After applying pressures of 2 and 5 Pa, as shown in Table III, there was a substantial decrease in the number of atoms reaching the substrate, with approximately 50 % and 75 % of the total number of ejected atoms, respectively, and a significant decrease in their energies.

TABLE III. The total number of material atoms arrived in the substrate depending on the pressure with argon gas ions bombardment.

Temperature	Materials	Total number of atoms
0.5 Pa	Si	38315
	Ge	33914
	Cu	37520
2 Pa	Si	19786
	Ge	14050
	Cu	14934
5 Pa	Si	8651
	Ge	6114
	Cu	7581

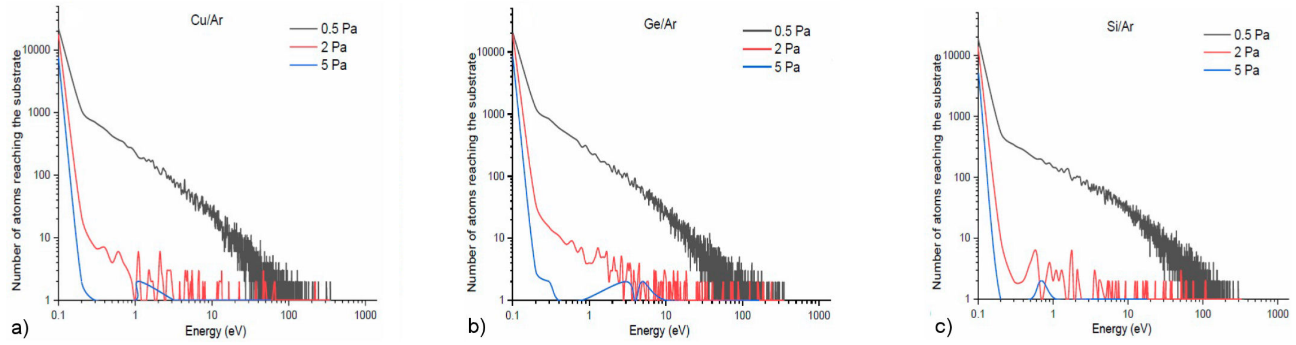

FIGURE 6. Number of arriving atoms as a function of the atom's kinetic energy for three different pressures $P = [0.5 \text{ Pa}, 2 \text{ Pa}, 5 \text{ Pa}]$ with Argon gas bombardment for a) Cu, b) Ge, and c) Si.

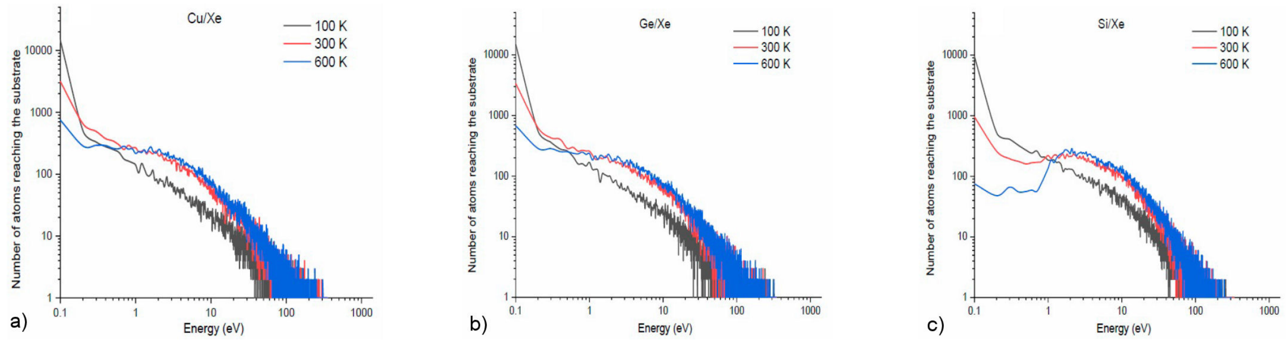

FIGURE 7. Number of arriving atoms as a function of the atom's kinetic energy using three different temperatures $T = [100, 300, \text{ and } 600 \text{ K}]$ with Xenon gas bombardment for a) Cu, b) Ge, and c) Si.

Low pressure inside the vacuum chamber will cause minor collisions between the particles; therefore, the ejected atoms will have a free path to reach the substrate.

4.2.3. Variation of temperature with a fixed pressure for Xenon ions

The same procedure will be carried out; temperature range $T = [100, 300, \text{ and } 600 \text{ K}]$ and 0.5 Pa as a static vacuum chamber pressure; the only difference is that we will now be using xenon instead of argon as the bombardment gas.

Replacing argon with xenon as the vacuum chamber gas and applying the same procedure described in Sec. 4.2.1, the results shown in Figs. 7a)-c) indicate a considerable decrease in the number of atoms arriving on the substrate. For example, an applied temperature of 100 K yields approximately 28000 atoms for Si compared to 38000 for argon. Almost the same phenomenon occurs in other materials (Ge and Cu). Xenon ions are known for their high bombardment energies, which provide a massive number of atoms ejected and a good sputtering yield. However, these can cause reflection or trajectory changes in the ejected particles when they collide with those of Xe, so they will not be able to travel to the substrate. Therefore, we must always choose a target compatible with the chosen gas.

As shown in Table IV, increasing the temperature increased the total number of particles arriving at the final destination (substrate).

TABLE IV. The total number of material atoms arrived in the substrate depending on temperature with Xenon gas ions bombardment.

Temperature	Materials	Total number of atoms
100 K	Si	38315
	Ge	33914
	Cu	37520
300 K	Si	39146
	Ge	35549
	Cu	36177
600 K	Si	41886
	Ge	37315
	Cu	38520

4.2.4. Variation of pressure with a fixed temperature for Xenon ions

As in Sec. 4.1.2, three different pressures $P = [0.5, 2{,}5 \text{ Pa}]$ and 100 K, were used as a fixed vacuum chamber temperature. Xenon replaces the argon gas used in the vacuum.

In the above figures (Figs. 8a)-c)), we can see that the application of xenon gas yields the same result as argon, except that the number of atoms that arrive at the substrate is dramatically diminished. As shown in Table V, for an applied pressure of 0.5 Pa, 28000 compared to 38000 for Si and

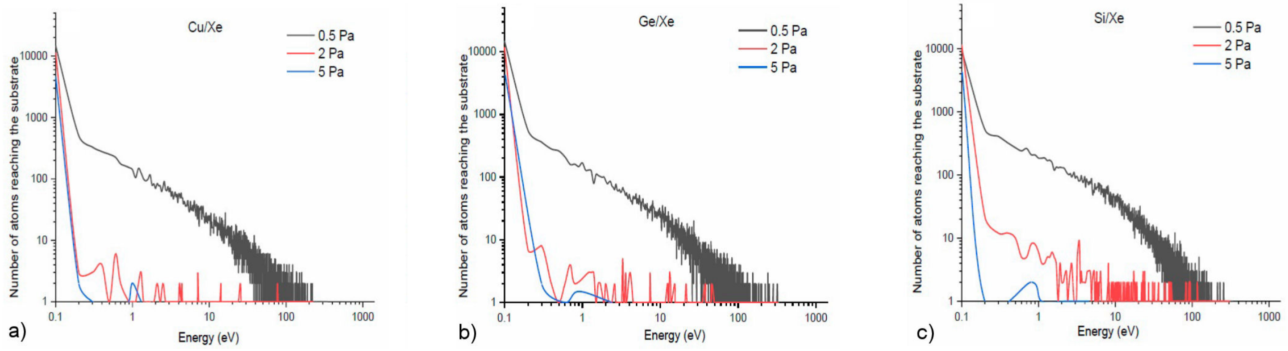

FIGURE 8. Number of arriving atoms as a function of the atom's kinetic energy for three different pressures $P = [0.5$ Pa, 2 Pa, 5 Pa$]$ with Xenon gas bombardment for a) Si, b) Ge, and c) Cu.

TABLE V. The total number of materials atoms arrived in the substrate depending on pressures with Xenon gas ions bombardment.

Temperature	Materials	Total number of atoms
0.5 Pa	Si	28141
	Ge	26940
	Cu	27676
2 Pa	Si	12224
	Ge	11571
	Cu	11987
5 Pa	Si	5103
	Ge	4628
	Cu	4986

approximately 26000, and 27000 compared with 34000 and 37000 for Ge and Cu, respectively.

When the pressure of 0.5 Pa was applied, the results proved that a large number of atoms arrived at the substrate compared to 2 and 5 Pa. In addition, most of these atoms arrived with energies in the range of $0.1 - 1$ eV, as seen in Fig. 8, where the higher energy tail extends up to 100 eV but contains relatively few atoms. The findings, as mentioned earlier, are crucial since it is seen that energetic bombardment influences the characteristics, stress, microstructure, and surface roughness of the deposited films [32, 56]. Therefore, high pressure considerably affected the morphology of the formed thin films, with a notable reduction in thickness and quality.

The SIMTRA simulation results were consistent with those reported in Refs. [32, 57–60] regarding the impact of various vacuum chamber gas parameters on the kinetic energy of ejected atoms reaching the substrate.

4.3. Comparison between materials

To define the best parameters for improving the growth and quality of thin films, we compared the studied materials (Si, Ge, and Cu) for each influencing parameter.

According to the figures above (Figs. 9-11), the obtained results are as follows:

1. Si material gives the best result for arriving at the substrate atom numbers, followed by Cu and Ge in the last position, although Cu has the best sputtering yield. This implies that the Si semiconductor has better deposition efficiency than the other materials.

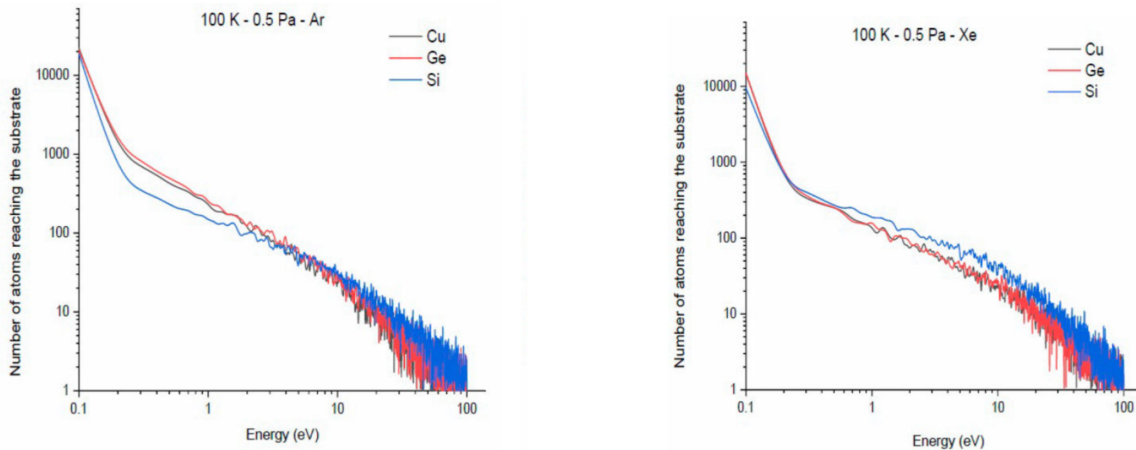

FIGURE 9. Comparison between arriving Si, Ge, and Cu atoms as a function of the atom's kinetic energy for 0.5 Pa and 100 K for a) Argon and b) xenon.

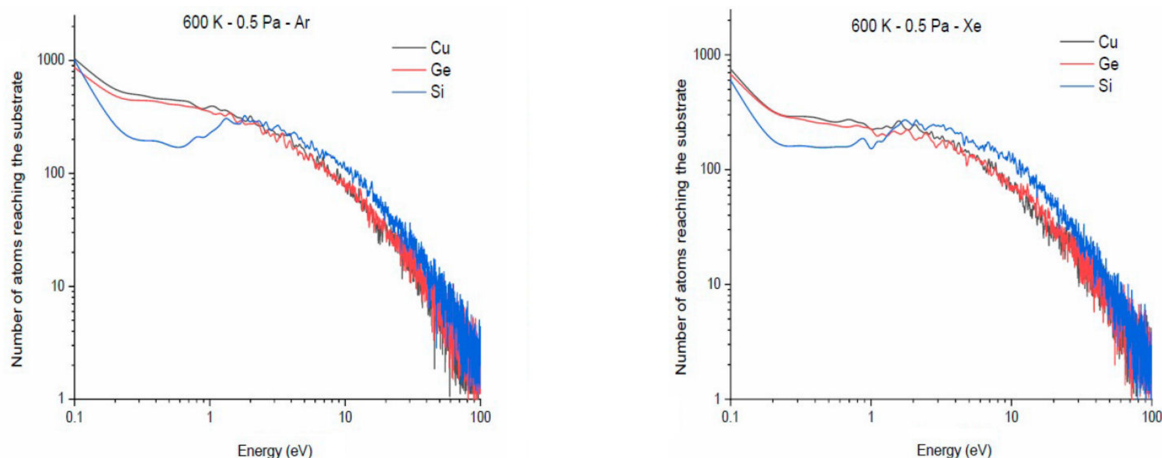

FIGURE 10. Comparison between arriving Si, Ge, and Cu atoms as a function of the atom's kinetic energy for 0.5 Pa and 600 K for a) Argon and b) xenon.

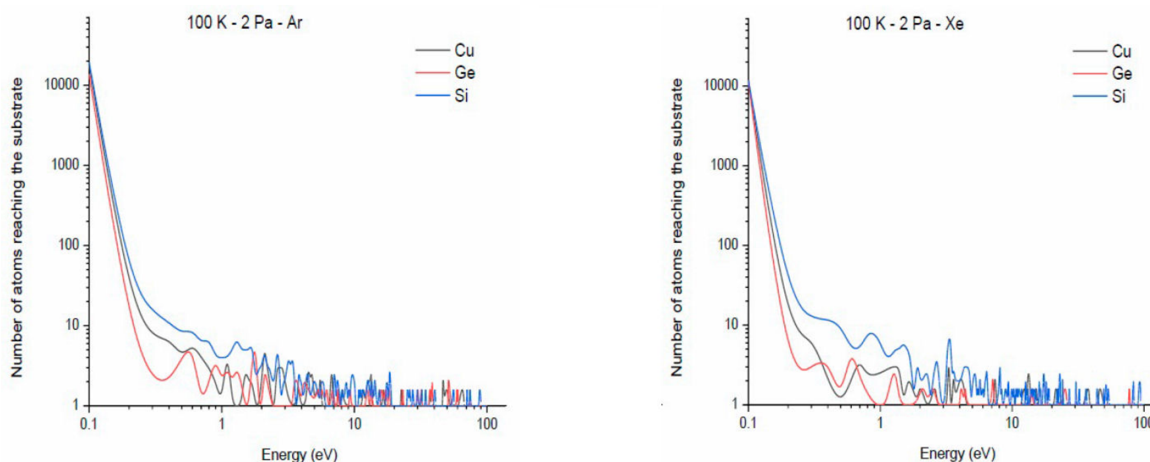

FIGURE 11. Comparison between arriving Si, Ge, and Cu atoms as a function of the atom's kinetic energy for 2 Pa and 100 K for a) Argon and b) xenon.

2. The desired thin films could be obtained at a low vacuum chamber pressure (in our case, 0.5 Pa).

3. In contrast, higher temperatures achieve the most important atom numbers at the substrate level. However, a severe amount arrives with high energy, which risks damaging the substrate or influencing the morphology of the film obtained.

5. Conclusion

The techniques for the deposition and coating of thin films are still in progress. However, deposition sputtering is one of the best-known methods to achieve the sound and desired quality of thin layers, depending on several factors.

Using the Monte Carlo codes such as SRIM and SIMTRA software described in this work allowed us to investigate the influence of temperature and high pressure on the magnetron sputtering process. We simulated several cases considering three materials (Si, Ge, and Cu) and two different bombardment gases (Ar and Xe) under temperature and high-pressure variations.

These findings demonstrate that the film characteristics are significantly influenced by the transport of sputtered atoms during the sputtering process. The acquired results are proven to help comprehend the impact of process parameters on transport and, as a result, in comprehending the sputter deposition process and the resulting film composition. They provided the following important information regarding the deposition of thin films:

– The increase in gas energy influences the atomic bonds of the materials, which leads to a significant difference between the ejected particles of metal (Cu) and semiconductors (Ge and Si).

– The increasing temperature values offer more kinetic energy to the particles, increasing their mobility inside the vacuum chamber and helping a large number of ejected atoms reach the substrate.

– The most important ejected atom number was determined when higher temperatures were applied. Nevertheless, the large number of atoms reaching the substrate when a high temperature is applied does not imply the obtention of the best thin film quality, awing that an essential number of atoms reaching the substrate with the highest energies (more than 20 eV) can ultimately damage the substrate structure or reflect, collide again with the ejected atoms or with the molecules of the gas, and influence the progress of the sputtering process. Low energies (in the range of 0.1 to 1 eV) were appropriate for building the finest films.

– In contrast, increasing the pressure from 0.5 to 5 Pa diminishes the particle's kinetic energy and hinders their movement by creating more collisions and a reduced mean-free path for a significant number of ejected particles to reach the substrate and directly influencing the aspect of the thin film.

– Eventually, the plasma gas injected into the vacuum chamber was considered harmful. The wrong choice of gas will decrease the number of atoms arriving at the substrate.

– Argon is the plasma gas used to deposit thin films by sputtering rather than xenon in experiments and industries for the following reasons:

   a. Argon (Ar) is a noble gas recovered from the air, but its concentration is much higher (0.93%) and is not considered rare. Xenon (Xe) which comes under "rare gas", is also a noble gas that can be obtained from air. Still, the economics of isolating them in air separation units depends on demand and pricing; their concentration in air is less than 20 parts per million (ppm).

   b. When using xenon for sputtering, the ejected atoms from the target are approximately 40% more than argon, but most of them leave it with higher energy. Even if they collide with plasma particles, they reach the substrate with significant energy. Some are returned to the plasma, where others penetrate, resulting in lower film quality owing to less particle deposition than argon.

Adding this work to our previous studies, we can contribute to the thin film deposition field by optimizing those fundamental parameters (vacuum chamber gas, bombardment energy, incidence angle, target-substrate distance, gas pressure, and temperature) in the disposition of research and researchers.

---

1. A. Bouazza, A. settaouti, Monte Carlo simulation of the influence of pressure and target-substrate distance on the sputtering process for metal and semiconductor layers, *Mod. Phys. Lett. B*. **30** (2016) 1650253, https://doi.org/10.1142/S0217984916502535.
2. A. Bouazza, A. settaouti, Study and simulation of the sputtering process of material layers in plasma, *Monte Carlo Methods Appl*. **22** (2016) 149, https://doi.org/10.1515/mcma-2016-0106.
3. A. Bouazza, A. settaouti, Understanding the contribution of energy and angular distribution in the morphology of thin films using Monte Carlo simulation, *Monte Carlo Methods Appl.* **24** (2018) 215, https://doi.org/10.1515/mcma-2018-0019.
4. S. E. C. Refas, A. Bouazza, and Y. Belhadji, 3D sputtering simulations of the CZTS, Si and CIGS thin films using Monte-Carlo method, *Monte Carlo Methods Appl.* **27** (2021) 373, https://doi.org/10.1515/mcma-2021-2094.
5. A. Bouazza, Sputtering of semiconductors, conductors, and dielectrics for the realization of electronics components thin-films, *International Journal of Thin Film Science and Technology*. **11** (2022) 225, https://doi.org/10.18576/ijtfst/110210.
6. C. A. Hernández-Gutiérrez *et al.*, The role of SnO2 high resistivity transparent layer deposited onto commercial conducting glass as front contact in superstrate configuration thin films solar cells technology: influence of the deposition technique., *Rev. Mex. Fis.* **65** (2019) 554, https://doi.org/10.31349/RevMexFis.65.554.
7. H. A. Macleod, Recent developments in deposition techniques for optical thin films and coatings, *Optical Thin Films and Coatings*. (2018) 3, https://doi.org/10.1016/B978-0-08-102073-9.00001-1.
8. S. Bairagi, K. Järrendahl, F. Eriksson, L. Hultman, J. Birch, and C.L. Hsiao, Glancing angle deposition and growth mechanism of inclined AlN nanostructures using reactive magnetron sputtering, *Coatings*. **10** (2020) 768, https://doi.org/10.3390/coatings10080768.
9. A. Bouazza, Simulation of the Deposition of Thin-Film Materials Used in the Manufacturing of Devices with Miniaturized Circuits. *J. Surf. Investig*. **16** (2022) 1221. https://doi.org/10.1134/S1027451022060283.
10. R. Tang *et al.*, Controlled sputtering pressure on high-quality Sb2Se3 thin film for substrate configurated solar cells, *Nanomaterials*. **10** (2020) 574, https://doi.org/10.3390/nano10030574.
11. N. Akcay, N. A. Sonmez, E. P. Zaretskaya, and S. Ozcelik, Influence of deposition pressure and power on characteristics of RF-Sputtered Mo films and investigation of sodium diffusion in the films, *Current Applied Physics.* **18** (2018) 491, https://doi.org/10.1016/j.cap.2018.02.014.
12. T. Li *et al.*, Influence of pressure on the properties of AlN deposited by DC reactive magnetron sputtering on Si (100)

substrate, *Micro and Nano Letters*. **14** (2019) 146, https://doi.org/10.1049/mnl.2018.5293.

13. X. Q. Tan, J. Y. Liu, J. R. Niu, J. Y. Liu, and J. Y. Tian, Recent progress in magnetron sputtering technology used on fabrics, *Materials*. **11** (2018) 1953, https://doi.org/10.3390/ma11101953.

14. M. Zubkins, H. Arslan, L. Bikse, and J. Purans, High power impulse magnetron sputtering of Zn/Al target in an Ar and Ar/O2 atmosphere: The study of sputtering process and AZO films, *Surface and coatings technology*. **369** (2019) 156, https://doi.org/10.1016/j.surfcoat.2019.04.044.

15. X. Hao *et al.*, Constructing multifunctional interphase between and Li metal by magnetron sputtering for highly stable solid-state lithium metal batteries, *Advanced Energy Materials.* **9** (2019) 1901604, https://doi.org/10.1002/aenm.201901604.

16. M. Qadir, Y. Li, and C. Wen, Ion-substituted calcium phosphate coatings by physical vapor deposition magnetron sputtering for biomedical applications: *A review, Acta biomaterialia*. **89** (2019) 14, https://doi.org/10.1016/j.actbio.2019.03.0064.

17. J. F. Ziegler, M. D. Ziegler, and J. P. Biersack, SRIM-The stopping and range of ions in matter, *Nuclear Instruments and Methods in Physics Research Section B: Beam Interactions with Materials and Atoms.* **268** (2010) 1818, https://doi.org/10.1016/j.nimb.2010.02.091.

18. U. Saha, K. Devan, and S. Ganesan, A study to compute integrated dpa for neutron and ion irradiation environments using SRIM-2013, *Journal of Nuclear Materials*. **503** (2018) 30, https://doi.org/10.1016/j.jnucmat.2018.02.039.

19. V. I. Shulga, Note on the artefacts in SRIM simulation of sputtering, *Applied Surface Science*. **439** (2018) 456, https://doi.org/10.1016/j.apsusc.2018.01.039.

20. J. Wang, M. B. Toloczko, N. Bailey, F.A. Garner, J. Gigax, and L. Shao, Modification of SRIM-calculated dose and injected ion profiles due to sputtering, injected ion buildup and void swelling, *Nuclear Instruments and Methods in Physics Research Section B: Beam Interactions with Materials and Atoms.* **387** (2016) 20, ttps://doi.org/10.1016/j.nimb.2016.09.015.

21. W. Möller, and W. Eckstein, Tridyn-A TRIM simulation code including dynamic composition changes, *Nuclear Instruments and Methods in Physics Research Section B: Beam Interactions with Materials and Atoms*. **2** (1984) 814, https://doi.org/10.1016/0168-583X(84)90321-5.

22. K. Van Aeken, S. Mahieu, and D. Depla, The metal flux from a rotating cylindrical magnetron: a Monte Carlo simulation, *Journal of Physics D: Applied Physics.* **41** (2008) 205307, https://doi.org/10.1088/0022-3727/41/20/205307.

23. J. O. Achenbach, S. Mráz, D. Primetzhofer, and J. M. Schneider, Correlative experimental and theoretical investigation of the angle-resolved composition evolution of thin films sputtered from a compound Mo2BC target, *Coatings*. **9** (2019) 206, https://doi.org/10.3390/coatings9030206.

24. M. Mickan, U. Helmersson, and D. Horwat, Effect of substrate temperature on the deposition of Al-doped ZnO thin films using high power impulse magnetron sputtering, *Surface and Coatings Technology.* **347** (2018) 245, https://doi.org/10.1016/j.surfcoat.2018.04.089.

25. F. Moens, I. C. Schramm, S. Konstantinidis, and D. Depla, On the microstructure of magnesium thin films deposited by magnetron sputtering, *Thin Solid Films.* **689** (2019) 137501, https://doi.org/10.1016/j.tsf.2019.137501.

26. N. Nedfors *et al.*, The influence of pressure and magnetic field on the deposition of epitaxial TiBx thin films from DC magnetron sputtering, *Vacuum.* **177** (2020) 109355, https://doi.org/10.1016/j.vacuum.2020.109355.

27. C. Oh *et al.*, Influence of oxygen partial pressure in In-Sn-Ga-O thin-film transistors at a low temperature, *Journal of Alloys and Compounds*. **805** (2019) 211, https://doi.org/10.1016/j.jallcom.2019.07.091.

28. P. C. Huang, C. H. Huang, M. Y. Lin, C. Y. Chou, C. Y. Hsu, and C. G. Kuo, The effect of sputtering parameters on the film properties of molybdenum back contact for CIGS solar cells, *International Journal of Photoenergy.* **2013** (2013) 390824, https://doi.org/10.1155/2013/390824.

29. S. H. Kim, Y. L. Choi, Y. S. Song, D. Y. Lee, and S. J. Lee, Influence of sputtering parameters on microstructure and morphology of TiO2 thin films, *Materials letters.* **57** (2002) 343, https://doi.org/10.1016/S0167-577X(02)00788-7.

30. Z. Bi, Z. Zhang, and P. Fan, Effect of sputter deposition parameters on the characteristics of PZT ferroelectric thin films, *Journal of Physics: Conference Series.* **61** (2007) 24, https://doi.org/10.1088/1742-6596/61/1/024.

31. W. Khan, Q. Wang, X. Jin, and T. Feng, The effect of sputtering parameters and doping of copper on surface free energy and magnetic properties of iron and iron nitride nano thin films on polymer substrate, *Materials.* **10** (2017) 217, https://doi.org/10.3390/ma10020217.

32. A. Settaouti, and L. Settaouti, Simulation of the transport of sputtered atoms and effects of processing conditions, *Applied surface science*. **254** (2008) 5750, https://doi.org/10.1016/j.apsusc.2008.03.042.

33. A. Bouazza, Deposition of Thin Films Materials used in Modern Photovoltaic Cells, *International Journal of Thin Film Science and Technology* **11** (2022) 313, https://doi.org/10.18576/ijtfst/110308.

34. D. Depla, and W. P. Leroy, Magnetron sputter deposition as visualized by Monte Carlo modeling, *Thin Solid Films*. **520** (2012) 6337, https://doi.org/10.1016/j.tsf.2012.06.032.

35. S. Mahieu, G. De Winter, D. Depla, R. De Gryse, and J. Denul, A model for the development of biaxial alignment in yttria stabilized zirconia layers, deposited by unbalanced magnetron sputtering, *Surface and Coatings Technology*. **187** (2004) 122, https://doi.org/10.1016/j.surfcoat.2004.01.008.

36. S. Mahieu, P. Ghekiere, G. De Winter, R. De Gryse, D. Depla, and O. I. Lebedev, Biaxially aligned Yttria Stabilized Zirconia and Titanium Nitride layers deposited by

unbalanced magnetron sputtering, *Solid State Phenomena*. **105** (2005) 447, https://doi.org/10.4028/www.scientific.net/SSP.105.447.

37. P. Ghekiere, S. Mahieu, G. De Winter, R. De Gryse, and D. Depla, Influence of the deposition parameters on the biaxial alignment of MgO grown by unbalanced magnetron sputtering, *Journal of crystal growth*. **271** (2004) 462, https://doi.org/10.1016/j.jcrysgro.2004.08.010.
38. S. Mahieu, G. Buyle, D. Depla, S. Heirwegh, P. Ghekiere, and R. De Gryse, Monte Carlo simulation of the transport of atoms in DC magnetron sputtering, *Nuclear Instruments and Methods in Physics Research Section B: Beam Interactions with Materials and Atoms.* **243** (2006) 313, https://doi.org/10.1016/j.nimb.2005.09.018.
39. A. Baptista, F. Silva, J. Porteiro, J. Míguez, and G. Pinto, Sputtering physical vapour deposition (PVD) coatings: A critical review on process improvement and market trend demands, *Coatings.* **8** (2018) 402, https://doi.org/10.3390/coatings8110402.
40. B. Rother, G. Ebersbach, and H. M. Gabriel, Substrate-rotation systems and productivity of industrial PVD processes, *Surface and Coatings Technology.* **116** (1999) 694, https://doi.org/10.1016/S0257-8972(99)00120-6.
41. C. G. Granqvist, Preparation of thin films and nanostructured coatings for clean tech applications: A primer, *Solar Energy Materials and Solar Cells*. **99** (2012) 166, https://doi.org/10.1016/j.solmat.2011.11.048.
42. V. S. Voitsenya *et al.*, Effect of sputtering on self-damaged recrystallized W mirror specimens, *Journal of nuclear materials*. **434** (2013) 375, https://doi.org/10.1016/j.jnucmat.2012.12.007.
43. H. C. Barshilia, A. Ananth, J. Khan, and G. Srinivas, Ar+ H2 plasma etching for improved adhesion of PVD coatings on steel substrates, *Vacuum*. **86** (2012) 1165, https://doi.org/10.1016/j.vacuum.2011.10.028.
44. P. A. Steinmann, and H. E. Hintermann, Adhesion of TiC and Ti (C, N) coatings on steel, *Journal of Vacuum Science and Technology A: Vacuum, Surfaces, and Films*. **3** (1985) 2394, https://doi.org/10.1116/1.572845.
45. H. van Lente, and J. I. van Til, Articulation of sustainability in the emerging field of nanocoatings, *Journal of Cleaner Production*. **16** (2008) 967, https://doi.org/10.1016/j.jclepro.2007.04.020.
46. G. Hobler, R. M. Bradley, and H. M. Urbassek, Probing the limitations of Sigmund's model of spatially resolved sputtering using Monte Carlo simulations, *Physical Review B*. **93** (2016) 205443, https://doi.org/10.1103/PhysRevB.93.205443.
47. H. Hofsäss, and O. Bobes, Prediction of ion-induced nanopattern formation using Monte Carlo simulations and comparison to experiments, *Applied Physics Reviews.* **6** (2019) 021307, https://doi.org/10.1063/1.5043188.
48. T. Smy *et al.*, Three-dimensional simulation of film microstructure produced by glancing angle deposition, *Journal of Vacuum Science and Technology A: Vacuum, Surfaces, and Films*. **18** (2000) 2507, https://doi.org/10.1116/1.1286394.
49. P. Meakin, and J. Krug, Three-dimensional ballistic deposition at oblique incidence, *Physical Review A*. **46** (1992) 3390, https://doi.org/10.1103/PhysRevA.46.3390.
50. A. Siad, A. Besnard, C. Nouveau, and P. Jacquet, Critical angles in DC magnetron glad thin films, *Vacuum*. **131** (2016) 305, https://doi.org/10.1016/j.vacuum.2016.07.012.
51. R. Mareus, C. Mastail, F. Anğay, N. Brunetière, and G. Abadias, Study of columnar growth, texture development and wettability of reactively sputter-deposited TiN, ZrN and HfN thin films at glancing angle incidence, *Surface and Coatings Technology.* **399** (2020) 126130, https://doi.org/10.1016/j.surfcoat.2020.126130.
52. G. Betz, and K. Wien, Energy and angular distributions of sputtered particles, *International Journal of Mass Spectrometry and Ion Processes*. **140** (1994) 1, https://doi.org/10.1016/0168-1176(94)04052-4.
53. O. M. Mattox, *Handbook of physical vapor deposition (PVD) processing*, William Andrew. (2010),
54. K. Seshan, (Ed.), *Handbook of thin film deposition,* William Andrew. (2012),
55. S. M. Rossnagel, Thin film deposition with physical vapor deposition and related technologies, *Journal of Vacuum Science and Technology A: Vacuum, Surfaces, and Films.* **21** (2003) 574, https://doi.org/10.1116/1.1600450.
56. S. M. Rossnagel, M. A. Russak, and J. J. Cuomo, Pressure and plasma effects on the properties of magnetron sputtered carbon films, *Journal of Vacuum Science and Technology A: Vacuum, Surfaces, and Films*. **5** (1987) 2150, https://doi.org/10.1116/1.574941.
57. S. N. Sambandam, S. Bhansali, V. R. Bhethanabotla, and D. K. Sood, Studies on sputtering process of multicomponent Zr-Ti-Cu-Ni-Be alloy thin films, *Vacuum.* **80** (2006) 406, https://doi.org/10.1016/j.vacuum.2005.07.037.
58. S. Mahieu, G. Buyle, D. Depla, S. Heirwegh, P. Ghekiere, and R. De Gryse, Monte Carlo simulation of the transport of atoms in DC magnetron sputtering, *Nuclear Instruments and Methods in Physics Research Section B: Beam Interactions with Materials and Atoms*. **243** (2006) 313, https://doi.org/10.1016/j.nimb.2005.09.018.
59. S. Kadlec, C. Quaeyhaegens, G. Knuyt, and L. M. Stals, Energy distribution of ions in an unbalanced magnetron plasma measured with energy-resolved mass spectrometry, *Surface and Coatings Technology.* **89** (1997) 177, https://doi.org/10.1016/S0257-8972(96)03088-5.
60. Z. L. Liu, L. Yu, K. L. Yao, X. B. Jing, X. A. Li, and X. Z. Sun, Kinetic Monte Carlo simulation of deposition of energetic copper atoms on a Cu (001) substrate, *Journal of Physics D: Applied Physics*. **28** (2005) 4202, https://doi.org/10.1088/0022-3727/38/23/010.